

# A New Family of Regularized Kernels for the Harmonic Oscillator

Benjamin W. Ong · Andrew J. Christlieb ·  
Bryan D. Quaife

Received: May 13, 2016

**Abstract** In this paper, we introduce a new family of regularized kernels, suitable for applying high-order time stepping to N-body systems. These high-order kernels are derived by a Taylor expansion of the non-regularized kernel about  $(r^2 + \epsilon^2)$ ; consequently, a sequence of increasingly accurate kernels can be derived. This paper proves the validity of the regularized kernels, constructs error estimates, and illustrates the benefits of using high-order kernels through numerical experiments.

**Keywords** Kernel regularization, singular integrals, N-body systems, high-order time stepping

**Mathematics Subject Classification (2000)** 65B99, 65P10, 70-08, 70F10, 70H05

## 1 Introduction

This paper is concerned with solutions to the system

$$\ddot{\mathbf{x}}_j = - \sum_{k \neq j} w_{jk} \nabla G(\mathbf{x}_j - \mathbf{x}_k), \quad (1)$$

---

Benjamin W. Ong  
Mathematical Sciences, Michigan Technological University, Houghton, MI, 49931  
ongbw@mtu.edu

Andrew J. Christlieb  
Dept. of Mathematics, Michigan State University, East Lansing, MI, 48824  
andrewch@msu.edu

Bryan D. Quaife  
Department of Scientific Computing, Florida State University, Tallahassee, FL, 32303  
bquaife@fsu.edu

where  $w_{jk}$  are constants, and  $G$  is the fundamental solution to Laplace's equation. Specifically,

$$G(r) = \begin{cases} -\frac{r}{2} & \text{in } \mathbb{R}^1, \\ -\frac{\ln r}{2\pi} & \text{in } \mathbb{R}^2, \\ \frac{1}{4\pi r} & \text{in } \mathbb{R}^3, \end{cases}$$

where  $r = \|\mathbf{x}\|_2$ . We write  $\|\cdot\|$  to mean  $\|\cdot\|_2$  from this point onwards. System (1), modulo a change in sign, arises in many dynamical systems such as the dynamics of charged particles [13], vortex dynamics [16, 25], and planetary motions [1]. By taking the first integral of system (1), we arrive at the Hamiltonian

$$H(\mathbf{x}, \dot{\mathbf{x}}) = \frac{1}{2} \sum_j \|\dot{\mathbf{x}}_j\|^2 + \sum_j \sum_{k \neq j} w_{jk} G(\mathbf{x}_j - \mathbf{x}_k), \quad (2)$$

which is a conserved quantity.

In numerical simulations, controlling the error in the Hamiltonian is of the utmost importance. Special classes of integrators, such as symplectic integrators [9, 21] or energy-conserving integrators [8], have been designed to help preserve either the symplectic structure of the equations (thereby adding stability and controlling the Hamiltonian error in some fashion as the simulation progresses), or explicitly conserving the Hamiltonian. If a fourth-order symplectic integrator [9] with a modest timestep is used to solve a 25-body problem in  $\mathbb{R}^2$  with  $w_{jk} = \pm 1$ , the error in the Hamiltonian rises quickly; in fact, each rise or dip corresponds to when particles cross each other (see Figure 1). A convergence study shows poor convergence to the true Hamiltonian for larger  $\Delta t$  before fourth-order convergence is observed for sufficiently small  $\Delta t$  (see Figure 1).

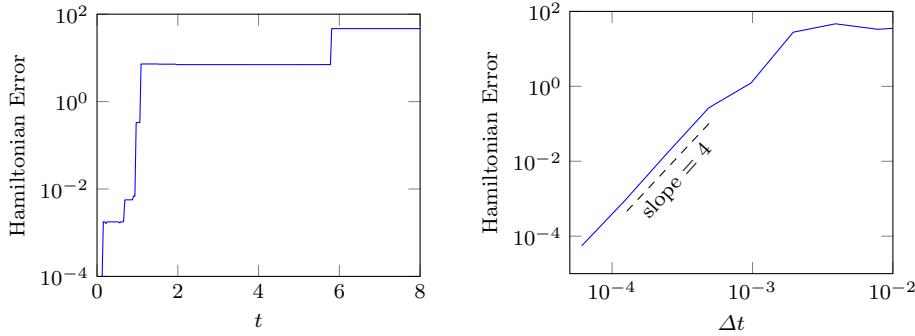


Fig. 1: *Left:* The Hamiltonian as a function of time when (1) is integrated with a fourth-order symplectic integrator with  $\Delta t = 3.91 \times 10^{-3}$ . *Right:* The error of the Hamiltonian at the time horizon  $T = 8$  for various time step sizes. The black line indicates fourth-order convergence.

A common way to overcome the reduced order of accuracy is to solve a regularized system instead of the original system,

$$\ddot{\mathbf{x}}_j = - \sum_{k \neq j} w_{jk} \nabla G^\epsilon(\mathbf{x}_j - \mathbf{x}_k). \quad (3)$$

which has the modified Hamiltonian

$$H^\epsilon(\mathbf{x}, \dot{\mathbf{x}}) = \frac{1}{2} \sum_j \|\dot{\mathbf{x}}_j\|^2 + \sum_j \sum_{k \neq j} w_{jk} G^\epsilon(\mathbf{x}_j - \mathbf{x}_k), \quad (4)$$

For example, the following algebraic regularization have been used in plasma and vortex simulations [5, 18],

$$G^\epsilon(r) = \begin{cases} -\frac{1}{2} \sqrt{r^2 + \epsilon^2} & \text{in } \mathbb{R}^1, \\ -\frac{\ln \sqrt{r^2 + \epsilon^2}}{2\pi} & \text{in } \mathbb{R}^2, \\ \frac{1}{4\pi} \frac{1}{\sqrt{r^2 + \epsilon^2}} & \text{in } \mathbb{R}^3. \end{cases} \quad (5)$$

In Figure 2, we use the same fourth-order symplectic integrator to solve the same 25-body system as before, except that we use  $G^\epsilon$  rather than  $G$  for two different values of  $\epsilon$ . The regularized system achieves fourth-order accuracy for large time step sizes. However for small time steps, the error stagnates; the value at which the error stagnates corresponds to the difference between the unregularized and regularized Hamiltonians,  $|H(0) - H^\epsilon(0)|$ . We shall refer to this difference as modelling error. This modelling error is observed in the left plot of Figure 2 at  $t = 0$ .

The modelling error can be reduced by decreasing  $\epsilon$ . However, this results in steeper derivatives of  $G^\epsilon(r)$ , creating larger jumps in the Hamiltonian error as two particles pass one another. The left plot of Figure 2 exactly demonstrates this behavior. The net effect, as can be seen in the right plot, is that smaller values of  $\epsilon$  require smaller time step sizes to achieve certain tolerances.

This paper seeks new regularizations that reduce modelling error while maintaining or relaxing the CFL condition. In Section 2, this new class of regularizations is introduced. In Section 3, we show that the Laplacian of the regularized potentials converges to the delta function, and we analyze the errors. In Section 4, we test the regularized potentials on the system (1) in one, two, and three dimensions. Finally, in Section 5, we summarize the results and discuss future work.

## 2 Regularized Kernels

Regularizations are a key tool in computing the evolution of Hamiltonian systems. One approach for forming a regularization, is to find a regularized fundamental solution by solving  $\mathcal{L}G^\epsilon = \delta_\epsilon$ , where  $\delta_\epsilon$  is a regularized approximation of the delta distribution, sometimes referred to as blob approximations [6, 7]. This has also been applied in other fields, for example in plasma physics [19], where a piecewise approximation to the delta function was introduced. The quality of different delta distribution regularizations has recently been analyzed in a functional analysis setting [12]. Alternatively, one can replace the fundamental solution with a

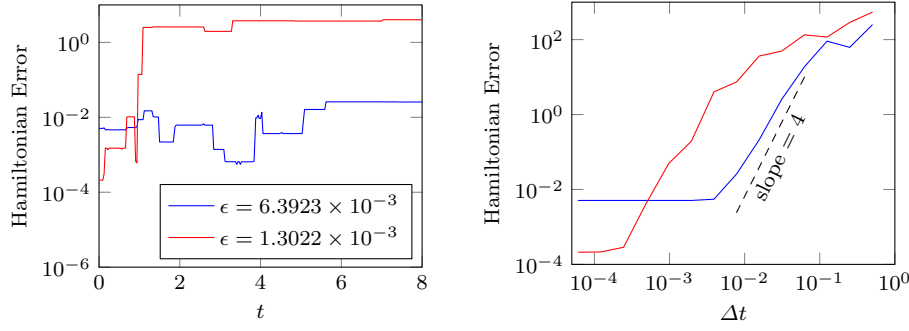


Fig. 2: *Left*: The Hamiltonian as a function of time when the regularized equation (3) is integrated with a fourth-order symplectic integrator with  $\Delta t = 3.91 \times 10^{-3}$ . Although a smaller  $\epsilon$  results in a smaller modelling error initially (at  $t = 0$ ), the steeper gradient in the kernel causes the time discretization error to dominate. *Right*: The error of the Hamiltonian at the time horizon  $T = 8$  for various time step sizes. The black line indicates fourth-order convergence.

regularized version. For example, a regularized fundamental solution might satisfy  $\Delta G^\delta(r) = n(\delta)\Delta G(r)s(r/\delta)$  [2], where  $s(r)$  is a shape function satisfying

$$s(r) = \text{erf}(r) - \frac{2}{\sqrt{\pi}}re^{-r^2},$$

sometimes referred to as a Gaussian mollifier, and  $n(\delta)$  is some normalizing factor that depends on the regularization  $\delta$ . Different filters or mollifiers can also be used [11]. Yet another approach is algebraic regularization, which was previously mentioned in the introduction. Algebraic regularization has been used in plasma physics [5, 10, 25], and for vortex sheet computations in fluid dynamics [16, 18, 24].

In this paper, a new family of algebraic regularized kernels is introduced. The regularized kernels are constructed by taking the binomial or Taylor expansion of the non-regularized kernels

$$G(r) = \begin{cases} -\frac{1}{2}(r^2 + \epsilon^2 - \epsilon^2)^{1/2} & \text{in } \mathbb{R}^1, \\ -\frac{1}{4\pi} \ln(r^2 + \epsilon^2) - \frac{1}{4\pi} \ln(1 - \epsilon^2(r^2 + \epsilon^2)^{-1}) & \text{in } \mathbb{R}^2, \\ \frac{1}{4\pi}(r^2 + \epsilon^2 - \epsilon^2)^{-1/2} & \text{in } \mathbb{R}^3, \end{cases}$$

and then truncating them after  $n$  terms

$$G^{\epsilon,n}(r) = \begin{cases} -\frac{1}{2} \sum_{i=0}^n \binom{\frac{1}{2}}{i} (-\epsilon^2)^i (r^2 + \epsilon^2)^{1/2-i} & \text{in } \mathbb{R}^1, \\ -\frac{1}{4\pi} \ln(r^2 + \epsilon^2) + \frac{1}{4\pi} \sum_{i=1}^n \frac{1}{i} \epsilon^{2i} (r^2 + \epsilon^2)^{-i} & \text{in } \mathbb{R}^2, \\ \frac{1}{4\pi} \sum_{i=0}^n \binom{-\frac{1}{2}}{i} (-\epsilon^2)^i (r^2 + \epsilon^2)^{-1/2-i} & \text{in } \mathbb{R}^3, \end{cases}$$

where  $\epsilon$  is the perturbation size. The generalized choose function is defined as

$$\binom{\alpha}{i} = \frac{(\alpha)_i}{i!} = \frac{1}{i!} \prod_{k=0}^{i-1} (\alpha - k),$$

where  $\alpha \in \mathbb{R}$  and  $(\alpha)_i$  is the falling factorial. By construction, for any  $\epsilon > 0$  and  $r \neq 0$ ,  $G^{\epsilon,n}(r) \rightarrow G(r)$  pointwise as  $n \rightarrow \infty$ . Note that when  $n = 0$ , the regularized kernel in equation (5) is recovered.

Before quantifying the error introduced by replacing  $G$  with  $G^{\epsilon,n}$ , we first show that  $G^{\epsilon,n}(\mathbf{x})$  tends to the fundamental solution for the Laplacian operator. Specifically, we will show that for any  $\epsilon > 0$ ,  $\Delta G^{\epsilon,n}(\mathbf{x}) \rightarrow \Delta G(\mathbf{x}) = -\delta(\mathbf{x})$  as  $n \rightarrow \infty$ , and that for any  $n$ ,  $\Delta G^{\epsilon,n}(\mathbf{x}) \rightarrow -\delta(\mathbf{x})$  as  $\epsilon \rightarrow 0$ , where  $\delta$  is the delta function, and all the convergences are understood to be taken in the weak sense. To check this convergence, we first show that  $\Delta G^{\epsilon,n}(\mathbf{x}) \rightarrow 0$  for all  $\mathbf{x} \neq 0$ , and that  $\int \Delta G^{\epsilon,n}(\mathbf{x}) d\mathbf{x}$  converges to  $-1$ . This implies that  $G^{\epsilon,n}(r)$  converges to the fundamental solution of the Laplacian operator.

*Remark 1* In general, if  $G^{\epsilon,n}(\mathbf{x})$  converges pointwise to  $G(\mathbf{x})$  for all  $\mathbf{x} \neq 0$ , then  $\Delta G^{\epsilon,n}$  converges weakly to the delta function. However, we will prove this result directly for our particular choice of  $G^{\epsilon,n}$  as this will lead to closed-form solutions of  $\Delta G^{\epsilon,n}$  which may be useful in future work.

We start by applying the Laplacian operator to the regularized kernel

$$\Delta G^{\epsilon,n}(r) = \begin{cases} -\sum_{i=0}^n \binom{\frac{1}{2}}{i} (-\epsilon^2)^i \left(\frac{1}{2} - i\right) (r^2 + \epsilon^2)^{-\frac{3}{2}-i} (-2ir^2 + \epsilon^2) & \text{in } \mathbb{R}^1, \\ -\frac{1}{\pi} \sum_{i=0}^n \epsilon^{2i} (r^2 + \epsilon^2)^{-i-2} (-ir^2 + \epsilon^2) & \text{in } \mathbb{R}^2, \\ -\frac{1}{2\pi} \sum_{i=0}^n \binom{-\frac{1}{2}}{i} (-\epsilon^2)^i \left(\frac{1}{2} + i\right) (r^2 + \epsilon^2)^{-\frac{5}{2}-i} (-2ir^2 + 3\epsilon^2) & \text{in } \mathbb{R}^3. \end{cases}$$

We can eliminate the generalized choose functions by using the identity

$$\binom{\frac{1}{2}}{i} \left(\frac{1}{2} - i\right) = \frac{(-1)^i \Gamma(i + \frac{1}{2})}{2\sqrt{\pi} \Gamma(i + 1)}.$$

Then in  $\mathbb{R}^1$ , the Laplacian operator of the regularized kernels is

$$\begin{aligned} \Delta G^{\epsilon,n}(r) &= -\frac{1}{2\sqrt{\pi}} \sum_{i=0}^n \frac{\Gamma(i + \frac{1}{2})}{\Gamma(i + 1)} \epsilon^{2i} (r^2 + \epsilon^2)^{-\frac{3}{2}-i} (-2ir^2 + \epsilon^2) \\ &= -\frac{1}{2\epsilon\sqrt{\pi}} \sum_{i=0}^n \frac{\Gamma(i + \frac{1}{2})}{\Gamma(i + 1)} \frac{(-2ia^2 + 1)}{(a^2 + 1)^{\frac{3}{2}+i}} \end{aligned}$$

where  $a = \frac{r}{\epsilon}$ . Similarly, using the identity

$$\binom{-\frac{1}{2}}{i} \left(\frac{1}{2} + i\right) = \frac{(-1)^i \Gamma(i + \frac{3}{2})}{\sqrt{\pi} \Gamma(i + 1)},$$

the Laplacian of the regularized kernels in  $\mathbb{R}^3$  is

$$\Delta G^{\epsilon,n}(r) = -\frac{1}{2\pi\sqrt{\pi}\epsilon^3} \sum_{i=0}^n \frac{\Gamma(i + \frac{3}{2})}{\Gamma(i+1)} \frac{(-2ia^2 + 3)}{(a^2 + 1)^{\frac{5}{2}+i}}.$$

We now give much simpler expressions for the Laplacian of these regularized Green functions that do not involve any summations.

**Theorem 1** *The Laplacian operator applied to the regularized kernels can be expressed as*

$$\Delta G^{\epsilon,n}(r) = \begin{cases} -\frac{1}{\epsilon\sqrt{\pi}} \left( \frac{1}{1+a^2} \right)^{n+\frac{3}{2}} \frac{\Gamma(n+\frac{3}{2})}{\Gamma(n+1)} & \text{in } \mathbb{R}^1, \\ -\frac{(n+1)}{\pi\epsilon^2} \left( \frac{1}{1+a^2} \right)^{n+2} & \text{in } \mathbb{R}^2, \\ -\frac{1}{\epsilon^3\pi\sqrt{\pi}} \left( \frac{1}{1+a^2} \right)^{n+\frac{5}{2}} \frac{\Gamma(n+\frac{5}{2})}{\Gamma(n+1)} & \text{in } \mathbb{R}^3, \end{cases} \quad (6)$$

where  $a = \frac{r}{\epsilon}$ .

*Proof* In  $\mathbb{R}^1$ , since  $\Gamma(z+1) = z\Gamma(z)$ , equation (6) holds for  $n = 0$ . Now, suppose equation (6) holds for  $n = p$ . Then,

$$\begin{aligned} \Delta G^{\epsilon,p+1}(r) &= -\frac{1}{\epsilon\sqrt{\pi}} \left( \frac{1}{1+a^2} \right)^{p+\frac{3}{2}} \frac{\Gamma(p+\frac{3}{2})}{\Gamma(p+1)} - \frac{\Gamma(p+\frac{3}{2})}{2\epsilon\sqrt{\pi}\Gamma(p+2)} \frac{(-2(p+1)a^2 + 1)}{(a^2 + 1)^{\frac{5}{2}+p}} \\ &= -\frac{1}{\epsilon\sqrt{\pi}} \left( \frac{1}{1+a^2} \right)^{p+\frac{5}{2}} \frac{\Gamma(p+\frac{3}{2})}{\Gamma(p+2)} \left[ (1+a^2) \frac{\Gamma(p+2)}{\Gamma(p+1)} + \frac{(-2(p+1)a^2 + 1)}{2} \right] \\ &= -\frac{1}{\epsilon\sqrt{\pi}} \left( \frac{1}{1+a^2} \right)^{p+\frac{5}{2}} \frac{\Gamma(p+\frac{3}{2})}{\Gamma(p+2)} \left[ (1+a^2)(p+1) + \frac{(-2(p+1)a^2 + 1)}{2} \right] \\ &= -\frac{1}{\epsilon\sqrt{\pi}} \left( \frac{1}{1+a^2} \right)^{p+\frac{5}{2}} \frac{\Gamma(p+\frac{3}{2})}{\Gamma(p+2)} \left( p + \frac{3}{2} \right) \\ &= -\frac{1}{\epsilon\sqrt{\pi}} \left( \frac{1}{1+a^2} \right)^{p+\frac{5}{2}} \frac{\Gamma(p+\frac{5}{2})}{\Gamma(p+2)}, \end{aligned}$$

which establishes that the equivalence must hold for  $n = p+1$ . A similar inductive argument can be used to establish equation (6) in  $\mathbb{R}^2$  and  $\mathbb{R}^3$ .

Now that we have a closed-form expression for the Laplacian of the regularized kernels, we can check that their weak limits converge to the delta function.

**Theorem 2** *The Laplacian of the regularized kernel  $G^{\epsilon,n}(r)$  converges weakly to the delta function. That is,*

$$\lim_{n \rightarrow \infty} \Delta G^{\epsilon,n}(r) = -\delta(r) \text{ for any } \epsilon > 0, \quad (7)$$

$$\lim_{\epsilon \rightarrow 0} \Delta G^{\epsilon,n}(r) = -\delta(r) \text{ for any } n \geq 0. \quad (8)$$

*Proof* We first check that the two limits (7) and (8) converge to 0 for all  $r \neq 0$ . If  $\epsilon > 0$  and  $r \neq 0$ , then, from equation (6),

$$\lim_{n \rightarrow \infty} \Delta G^{\epsilon, n}(r) = 0,$$

for  $\mathbb{R}^1, \mathbb{R}^2$  and  $\mathbb{R}^3$ . Next, since equation (6) can be rewritten as

$$\Delta G^{\epsilon, n}(r) = \begin{cases} -\frac{\epsilon^{2n+2}}{\sqrt{\pi}} \left( \frac{1}{\epsilon^2 + r^2} \right)^{n+\frac{3}{2}} \frac{\Gamma(n+\frac{3}{2})}{\Gamma(n+1)} & \text{in } \mathbb{R}^1, \\ -\frac{(n+1)\epsilon^{2n+2}}{\pi} \left( \frac{1}{\epsilon^2 + r^2} \right)^{n+2} & \text{in } \mathbb{R}^2, \\ -\frac{\epsilon^{2n+2}}{\pi\sqrt{\pi}} \left( \frac{1}{\epsilon^2 + r^2} \right)^{n+\frac{5}{2}} \frac{\Gamma(n+\frac{5}{2})}{\Gamma(n+1)} & \text{in } \mathbb{R}^3, \end{cases}$$

it follows that for any  $n \geq 0$ ,  $r \neq 0$ ,

$$\lim_{\epsilon \rightarrow 0} \Delta G^{\epsilon, n}(r) = 0.$$

Next, for all  $\epsilon$  and  $n$ ,

$$\begin{aligned} 2 \int_0^\infty -\frac{1}{\epsilon\sqrt{\pi}} \left( \frac{1}{1 + \frac{r^2}{\epsilon^2}} \right)^{n+\frac{3}{2}} \frac{\Gamma(n+\frac{3}{2})}{\Gamma(n+1)} dr &= -1, \quad \text{in } \mathbb{R}^1, \\ -\frac{n+1}{\pi\epsilon^2} \int_0^\infty \left( \frac{1}{1 + \frac{r^2}{\epsilon^2}} \right)^{n+2} 2\pi r dr &= -1, \quad \text{in } \mathbb{R}^2, \\ -\frac{1}{\epsilon^3\pi\sqrt{\pi}} \int_0^\infty \left( \frac{1}{1 + \frac{r^2}{\epsilon^2}} \right)^{n+\frac{5}{2}} \frac{\Gamma(n+\frac{5}{2})}{\Gamma(n+1)} 4\pi r^2 dr &= -1, \quad \text{in } \mathbb{R}^3. \end{aligned}$$

Finally, let  $f$  be a compactly supported smooth function and  $\epsilon > 0$ . Then, for any  $\alpha > 0$ ,

$$\int_{\mathbb{R}^d} \lim_{n \rightarrow \infty} \Delta G^{\epsilon, n}(\mathbf{x}) f(\mathbf{x}) d\mathbf{x} = \int_{B(0, \alpha)} \lim_{n \rightarrow \infty} \Delta G^{\epsilon, n}(\mathbf{x}) f(\mathbf{x}) d\mathbf{x}.$$

Since this holds for all  $\alpha > 0$ , we have

$$\begin{aligned} \int_{\mathbb{R}^d} \lim_{n \rightarrow \infty} \Delta G^{\epsilon, n}(\mathbf{x}) f(\mathbf{x}) d\mathbf{x} &= f(0) \int_{B(0, \alpha)} \lim_{n \rightarrow \infty} \Delta G^{\epsilon, n}(\mathbf{x}) d\mathbf{x} \\ &= f(0) \int_{\mathbb{R}^d} \lim_{n \rightarrow \infty} \Delta G^{\epsilon, n}(\mathbf{x}) d\mathbf{x} \\ &= -f(0), \end{aligned}$$

which establishes (7). The proof of (8) is similarly proved by fixing  $n > 0$  and showing that

$$\int_{\mathbb{R}^d} \lim_{\epsilon \rightarrow 0} \Delta G^{\epsilon, n}(\mathbf{x}) f(\mathbf{x}) d\mathbf{x} = -f(0).$$

### 3 Error Analysis

In this section we systematically analyze the modelling error arising from using regularized kernels in  $\mathbb{R}^1, \mathbb{R}^2$  and  $\mathbb{R}^3$ . The goal is to demonstrate that the new classes of kernels introduced in Section 2 can reduce the far field modelling error, while still allowing for large time steps of the Hamiltonian system (1).

#### 3.1 Error analysis of regularized Hamiltonians

The total error can be decomposed into two parts: the modelling error from replacing  $\nabla_{\mathbf{x}}G(\|\mathbf{x} - \mathbf{y}\|)$  with  $\nabla_{\mathbf{x}}G^{\epsilon,n}(\|\mathbf{x} - \mathbf{y}\|)$ , and the time stepping error associated with time stepping the regularized system. In particular, the error in the Hamiltonian (2) can be bounded as

$$|H^{\epsilon,n}(t) - H(0)| \leq |H^{\epsilon,n}(t) - H^{\epsilon,n}(0)| + |H^{\epsilon,n}(0) - H(0)|.$$

The first term is the time-stepping error,  $|H^{\epsilon,n}(t) - H^{\epsilon,n}(0)|$ , which depends on the chosen time step size. For  $\epsilon > 0$  and  $n \geq 0$ , the time stepping error goes to zero as  $\Delta t \rightarrow 0$ . The second term is the modelling or smoothing error, and satisfies

$$|H^{\epsilon,n}(0) - H(0)| = \sum_j \sum_{k \neq j} w_{jk} (G^{\epsilon,n}(\mathbf{x}_j - \mathbf{x}_k) - G(\mathbf{x}_j - \mathbf{x}_k)). \quad (9)$$

Since the force relies on the gradient of the fundamental solution, we investigate the error of the gradient. One way to quantify the quality of the regularization is to measure the *global smoothing error*,

$$e(\epsilon, n) = \begin{cases} 2 \int_0^\infty \left| \frac{\partial G^{\epsilon,n}(r)}{\partial r} - \frac{\partial G(r)}{\partial r} \right| dr & \text{in } \mathbb{R}^1, \\ \int_0^\infty \left| \frac{\partial G^{\epsilon,n}(r)}{\partial r} - \frac{\partial G(r)}{\partial r} \right| 2\pi r dr & \text{in } \mathbb{R}^2, \\ \int_0^\infty \left| \frac{\partial G^{\epsilon,n}(r)}{\partial r} - \frac{\partial G(r)}{\partial r} \right| 4\pi r^2 dr & \text{in } \mathbb{R}^3, \end{cases} \quad (10)$$

where the gradient of the regularized kernels are

$$\frac{\partial G^{\epsilon,n}(r)}{\partial r} = \begin{cases} -r \sum_{i=0}^n \binom{\frac{1}{2}}{i} (-\epsilon^2)^i \left(\frac{1}{2} - i\right) (r^2 + \epsilon^2)^{-1/2-i} & \text{in } \mathbb{R}^1, \\ -\frac{r}{2\pi} \sum_{i=0}^n \epsilon^{2i} (r^2 + \epsilon^2)^{-i-1} & \text{in } \mathbb{R}^2, \\ -\frac{r}{2\pi} \sum_{i=0}^n \binom{-\frac{1}{2}}{i} (-\epsilon^2)^i \left(-\frac{1}{2} - i\right) (r^2 + \epsilon^2)^{-3/2-i} & \text{in } \mathbb{R}^3. \end{cases}$$

It should be observed that if  $r = 0$ ,  $\frac{\partial G^{\epsilon,n}(r)}{\partial r} = 0$  which is consistent with the physical argument that a particle does not feel any self-force.

In Table 1, we report pairings  $(\epsilon, n)$  that result in same regularization error when truncating the infinite integral at 1. That is, we choose values  $(\epsilon, n)$  so that

$$\int_{B(0,1)} |\nabla G^{\epsilon,n} - \nabla G| = 10^{-2}, \quad (11)$$

where  $B(0, 1)$  is the unit ball centered at the origin in the appropriate dimension. These  $(\epsilon, n)$  pairings will be used for the numerical experiments in Section 4.



$n$	$\epsilon (\mathbb{R}^1)$	$\epsilon (\mathbb{R}^2)$	$\epsilon (\mathbb{R}^3)$
0	$1.0051 \times 10^{-2}$	$6.3923 \times 10^{-3}$	$5.0189 \times 10^{-3}$
1	$2.0001 \times 10^{-2}$	$1.2733 \times 10^{-2}$	$1.0001 \times 10^{-2}$
2	$2.6667 \times 10^{-2}$	$1.6977 \times 10^{-2}$	$1.3333 \times 10^{-2}$
4	$3.6572 \times 10^{-2}$	$2.3283 \times 10^{-2}$	$1.8286 \times 10^{-2}$
10	$5.6755 \times 10^{-2}$	$3.6132 \times 10^{-2}$	$2.8378 \times 10^{-2}$

Table 1: Values of  $\epsilon$  and  $n$  that result in a global smoothing error of  $10^{-2}$ . These pairings are used in Figures 3, 4, 6, 8, 10, 12, 15, and 17.

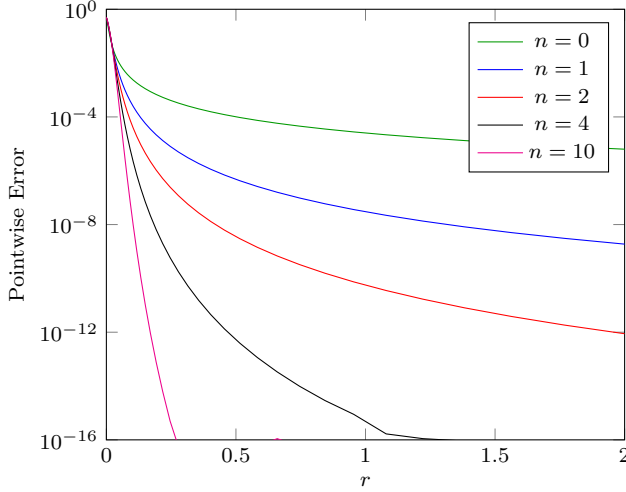


Fig. 3: Pointwise error in  $\mathbb{R}^1$  of  $\frac{\partial}{\partial r}(G^{\epsilon,n} - G)$  as a function of  $r$  for various  $(\epsilon, n)$  pairings. The integral of each of these error curves is kept fixed (Table 1).

### 3.2 Error Analysis in $\mathbb{R}^1$

The pointwise error in  $\mathbb{R}^1$  is

$$\begin{aligned} \frac{\partial}{\partial r} (G^{\epsilon,n}(r) - G(r)) &= \frac{\partial}{\partial r} \left( \sum_{i=n+1}^{\infty} \binom{\frac{1}{2}}{i} (-1)^i \epsilon^{2i} (r^2 + \epsilon^2)^{\frac{1}{2}-i} \right) \\ &= \sum_{i=n+1}^{\infty} 2r \left( \frac{1}{2} - i \right) \binom{\frac{1}{2}}{i} (-1)^i \epsilon^{2i} (r^2 + \epsilon^2)^{-\frac{1}{2}-i}. \end{aligned}$$

In Figure 3, the pointwise error at various  $r \in (0, 1)$  is plotted for various  $(\epsilon, n)$  pairings which all achieve a smoothing error (10) of  $10^{-2}$  (Table 1). We observe that by using larger values of  $n$ , the error in the far field is greatly reduced, at the expense of a slight increase in the error near the singularity.

To bound the global smoothing error, suppose all the point charges are contained in the interval  $[-R, R]$ . Then the error term of interest is

$$2 \int_0^R \rho(r) \frac{\partial}{\partial r} (G^{\epsilon,n}(r) - G(r)) dr.$$

The global smoothing error can be bounded as

$$\begin{aligned}
e[n, \epsilon] &= 2 \left| \int_0^R \rho(r) \frac{\partial}{\partial r} (G^{\epsilon, n}(r) - G(r)) dr, \right| \\
&\leq 2\rho_{max} \left| \int_0^R \frac{\partial}{\partial r} \left( \sum_{i=n+1}^{\infty} \binom{\frac{1}{2}}{i} (-1)^i \epsilon^{2i} (r^2 + \epsilon^2)^{\frac{1}{2}-i} \right) dr \right| \\
&= 2\rho_{max} \left| \left( \sum_{i=n+1}^{\infty} \binom{\frac{1}{2}}{i} (-1)^i \epsilon^{2i} (r^2 + \epsilon^2)^{\frac{1}{2}-i} \right) \right|_0^R \\
&= \epsilon \rho_{max} \left| 2 \sum_{i=n+1}^{\infty} \binom{\frac{1}{2}}{i} (-1)^i \left( \left( \frac{\epsilon^2}{R^2 + \epsilon^2} \right)^{i-\frac{1}{2}} - 1 \right) \right| \\
&=: \epsilon \rho_{max} |S[n, \epsilon]|.
\end{aligned}$$

If  $S[0, \epsilon] < \infty$  (which we show next), then  $\lim_{n \rightarrow \infty} S[n, \epsilon] = 0$ . This allows us to conclude:

- for  $\epsilon > 0$ ,  $\lim_{n \rightarrow \infty} e[n, \epsilon] = 0$ , since  $\lim_{n \rightarrow \infty} S[n, \epsilon] = 0$ .
- for  $0 < n < \infty$ ,  $\lim_{\epsilon \rightarrow 0} e[n, \epsilon] = 0$ , since  $S[n, \epsilon]$  is finite.

We now establish that  $S[0, \epsilon]$  is finite. By introducing the variable  $z = \frac{\epsilon^2}{R^2 + \epsilon^2} \in (0, 1)$ ,

$$\begin{aligned}
S[0, \epsilon] &= 2 \sum_{i=1}^{\infty} \binom{\frac{1}{2}}{i} (-1)^i \left( \left( \frac{\epsilon^2}{R^2 + \epsilon^2} \right)^{i-\frac{1}{2}} - 1 \right) \\
&= 2 \sum_{i=1}^{\infty} \binom{\frac{1}{2}}{i} (-1)^i (z^{i-\frac{1}{2}} - 1) \\
&= 2 \left( \frac{-\sqrt{z}}{1 + \sqrt{1-z}} + 1 \right).
\end{aligned}$$

Since this value is bounded for any  $\epsilon$  and  $R$ , we know that the global smoothing error in  $\mathbb{R}^1$  converges to zero by either decreasing  $\epsilon$  or by increasing  $n$ . More generally, we can provide an error estimate for the global smoothing error. Let  $g(z) = \frac{-2}{1 + \sqrt{1-z}}$ . Taylor's theorem tells us that

$$\left| 2 \sum_{i=n+1}^{\infty} \binom{\frac{1}{2}}{i} (-1)^i z^{i-1} \right| = \left| \frac{-2}{1 + \sqrt{1-z}} - 2 \sum_{i=1}^n \binom{\frac{1}{2}}{i} (-1)^i z^{i-1} \right| = \frac{|g^{(n)}(\xi)|}{n!} z^n,$$

where  $\xi \in [0, z]$ . Hence,

$$\left| 2 \sum_{i=n+1}^{\infty} \binom{\frac{1}{2}}{i} (-1)^i z^{i-\frac{1}{2}} \right| = \left| \frac{-2\sqrt{z}}{1 + \sqrt{1-z}} - 2 \sum_{i=1}^n \binom{\frac{1}{2}}{i} (-1)^i z^{i-\frac{1}{2}} \right| = \frac{|g^{(n)}(\xi)|}{n!} z^{n+\frac{1}{2}}.$$

Since

$$2 \sum_{i=1}^{\infty} \binom{\frac{1}{2}}{i} (-1)^i = -2,$$

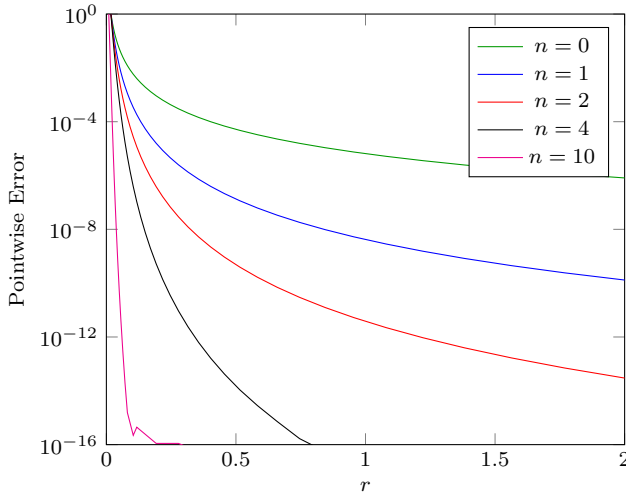


Fig. 4: Pointwise error in  $\mathbb{R}^2$  of  $\frac{\partial}{\partial r}(G^{\epsilon,n} - G)$  as a function of  $r$  for various  $(\epsilon, n)$  pairings (Table 1). The integral of each of these error curves is kept fixed.

this gives

$$2 \sum_{i=n+1}^{\infty} \binom{\frac{1}{2}}{i} (-1)^i = -2 - 2 \sum_{i=1}^n \binom{\frac{1}{2}}{i} (-1)^i.$$

This allows us to conclude that

$$\begin{aligned} e[n, \epsilon] = \epsilon \rho_{\max} |S[n, \epsilon]| &\leq \epsilon \rho_{\max} \left( \frac{|g^{(n)}(\xi)|}{n!} z^{n+\frac{1}{2}} + 2 \left( 1 + \sum_{i=1}^n \binom{\frac{1}{2}}{i} (-1)^i \right) \right) \\ &\leq \epsilon \rho_{\max} \left( \frac{|g^{(n)}(\xi)|}{n!} \left( \frac{\epsilon^2}{R^2 + \epsilon^2} \right)^{n+\frac{1}{2}} + 2 \left( 1 + \sum_{i=1}^n \binom{\frac{1}{2}}{i} (-1)^i \right) \right). \end{aligned}$$

### 3.3 Error Analysis in $\mathbb{R}^2$

The pointwise error in  $\mathbb{R}^2$  is

$$\frac{\partial}{\partial r} (G^{\epsilon,n}(r) - G(r)) = \frac{r}{2\pi} \sum_{i=n+1}^{\infty} \frac{1}{i} \epsilon^{2i} (r^2 + \epsilon^2)^{-i-1},$$

In Figure 4, the pointwise error at various  $r \in (0, 1)$  is plotted for various  $(\epsilon, n)$  pairings which all achieve a smoothing error of  $10^{-2}$  (Table 1). We observe that by using larger values of  $n$ , the error in the far field is greatly reduced, at the expense of a slight increase in the error near the singularity.

To bound the global smoothing error, suppose all the point charges are contained in a circle of radius  $R$ . Then,

$$\begin{aligned}
e[n, \epsilon] &= \left| \int_{\Omega} \rho(r, \theta) \frac{\partial}{\partial r} (G^{\epsilon, n}(r) - G(r)) d\Omega \right| \\
&\leq 2\pi \rho_{\max} \left| \int_0^R r \frac{\partial}{\partial r} (G^{\epsilon, n}(r) - G(r)) dr \right| \\
&= \rho_{\max} \left| \int_0^R \left( r^2 \sum_{i=n+1}^{\infty} \epsilon^{2i} (r^2 + \epsilon^2)^{-i-1} \right) dr \right| \\
&= \epsilon \rho_{\max} \left| \sum_{i=n+1}^{\infty} \frac{-(-1)^i \pi^{3/2}}{4\Gamma(-i + 3/2)i!} + \sum_{i=n+1}^{\infty} \left( \frac{\epsilon}{R} \right)^{2i-1} \frac{{}_2F_1 \left( i + \frac{1}{2}, i - \frac{1}{2}; i + \frac{1}{2}; -\frac{\epsilon^2}{R^2} \right)}{2i-1} \right| \\
&=: \epsilon \rho_{\max} |S[n, \epsilon]|.
\end{aligned}$$

Here,  ${}_2F_1(a, b; c; z)$  is the hypergeometric function defined as

$${}_2F_1(a, b; c; z) = \sum_{n=0}^{\infty} \frac{(a)_n (b)_n}{(c)_n} \frac{z^n}{n!},$$

where  $(a)_n = a(a-1)(a-2) \cdots (a-n+1)$  is the falling factorial,  $|z| < 1$ , and the function is analytically continued for  $|z| \geq 1$ . As was the case in  $\mathbb{R}^1$ , we are able to write the bound in the error as  $e(\epsilon, n) \leq \epsilon \rho_{\max} |S[n, \epsilon]|$ . Therefore, using the earlier argument, if  $S[0, \epsilon] < \infty$ , then the smoothing error goes to 0 as  $\epsilon$  goes to 0 or  $n$  goes to infinity.

We can partially simplify  $S[0, \epsilon]$  as

$$S[0, \epsilon] = \frac{\pi}{2} + \sum_{i=1}^{\infty} \frac{1}{2i-1} \left( \frac{z}{1-z} \right)^{i-\frac{1}{2}} {}_2F_1 \left( i + \frac{1}{2}, i - \frac{1}{2}; i + \frac{1}{2}; -\frac{z}{1-z} \right),$$

where  $z = \frac{\epsilon^2}{\epsilon^2 + R^2} \in (0, 1)$ . Unfortunately, unlike in  $\mathbb{R}^1$ , we are unable to form a closed-form expression for this summation. Therefore, we illustrate this function in Figure 5. As desired, this function is bounded for all  $z \in (0, 1)$ , and we can conclude that  $S[0, \epsilon]$  is finite. Therefore,  $e \rightarrow 0$  as  $\epsilon \rightarrow 0$  for a fixed  $n$ , and as  $n \rightarrow \infty$  for a fixed  $\epsilon$ . Since we do not have a closed-form expression for  $S[0, \epsilon]$ , we are unable to use Taylor's theorem to give an estimate of the smoothing error for any  $n$  and  $\epsilon$ . However, we can easily approximate  $S[n, \epsilon]$  since the infinite sum involving the hypergeometric function rapidly converges.

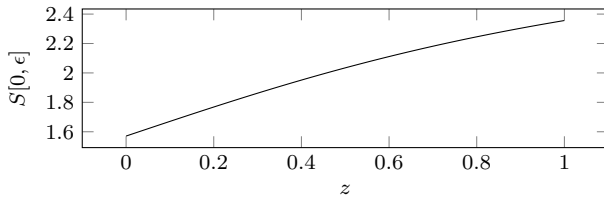


Fig. 5: The infinite sum  $S[0, \epsilon]$ . A bound for the smoothing error in  $\mathbb{R}^2$  is given by  $e[n, \epsilon] \leq \epsilon \rho_{\max} |S[0, \epsilon]|$ .

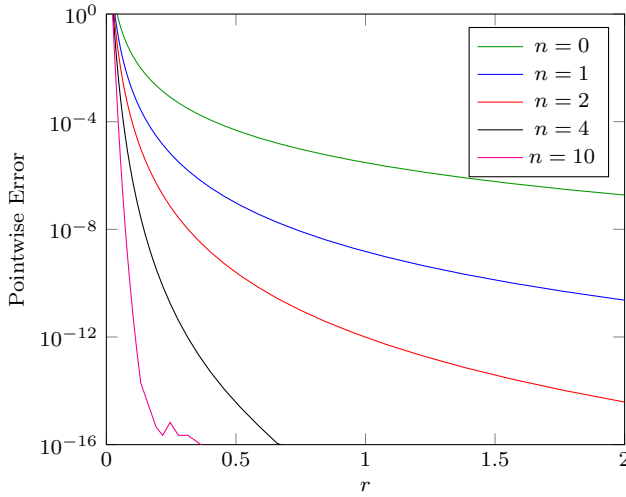


Fig. 6: Pointwise error in  $\mathbb{R}^3$  of  $\frac{\partial}{\partial r}(G^{\epsilon,n} - G)$  as a function of  $r$  for various  $(\epsilon, n)$  pairings (Table 1). The integral of each of these error curves is kept fixed.

### 3.4 Error Analysis in $\mathbb{R}^3$

The pointwise error satisfies

$$\frac{\partial}{\partial r}(G^{\epsilon,n}(r) - G(r)) = \frac{r}{2\pi} \sum_{i=n+1}^{\infty} \binom{-\frac{1}{2}}{i} (-\epsilon^2)^i \left(-\frac{1}{2} - i\right) (r^2 + \epsilon^2)^{-3/2-i}.$$

In Figure 6, the pointwise error at various  $r \in (0, 1)$  is plotted for various  $(\epsilon, n)$  pairings which all achieve a smoothing error of  $10^{-2}$  (Table 1). We observe that by using larger values of  $n$ , the error in the far field is greatly reduced, at the expense of a slight increase in the error near the singularity.

To bound the global smoothing error, suppose all the charges are contained in a ball of radius  $R$ , and let  $\rho$  be compactly supported in  $\Omega$ . Then,

$$\begin{aligned} e[n, \epsilon] &= \left| \int_{\Omega} \rho(r, \theta) \frac{\partial}{\partial r} (G^{\epsilon,n}(r) - G(r)) d\Omega \right| \\ &\leq 4\pi \rho_{\max} \left| \int_0^R r^2 \frac{\partial}{\partial r} (G^{\epsilon,n}(r) - G(r)) dr \right| \\ &= 2\rho_{\max} \left| \int_0^R \left( r^3 \sum_{i=n+1}^{\infty} \binom{-\frac{1}{2}}{i} (-\epsilon^2)^i \left(-\frac{1}{2} - i\right) (r^2 + \epsilon^2)^{-3/2-i} \right) dr \right| \\ &= \rho_{\max} \left| \int_{\epsilon^2}^{R^2 + \epsilon^2} \left( (u - \epsilon^2) \sum_{i=n+1}^{\infty} \binom{-\frac{1}{2}}{i} (-\epsilon^2)^i \left(-\frac{1}{2} - i\right) u^{-3/2-i} \right) du \right| \\ &= \epsilon \rho_{\max} \left| \sum_{i=n+1}^{\infty} \binom{-\frac{1}{2}}{i} (-1)^i \left\{ \frac{(-\frac{1}{2} - i)}{(\frac{1}{2} - i)} \left( \left( \frac{\epsilon^2}{R^2 + \epsilon^2} \right)^{i-\frac{1}{2}} - 1 \right) - \right. \right. \\ &\quad \left. \left. \left( \left( \frac{\epsilon^2}{R^2 + \epsilon^2} \right)^{i+\frac{1}{2}} - 1 \right) \right\} \right| \\ &=: \epsilon \rho_{\max} |S[n, \epsilon]|. \end{aligned}$$

The summation  $S[n, \epsilon]$  can be further simplified, by shifting sums and using standard properties of the generalized choose function, as

$$S[n, \epsilon] = \frac{2n+3}{2(n+1)} \binom{-\frac{1}{2}}{n} (-1)^n (z^{n+\frac{1}{2}} - 1) + \frac{1}{2} \sum_{i=n+1}^{\infty} \binom{-\frac{1}{2}}{i} (-1)^i \frac{1}{i+1} (z^{i+\frac{1}{2}} - 1),$$

where  $z = \frac{\epsilon^2}{\epsilon^2 + R^2} \in (0, 1)$ . Similar to  $\mathbb{R}^1$ , the infinite sum can be computed exactly as

$$S[0, \epsilon] = -2 + \frac{3z^{\frac{1}{2}}}{2} + \frac{z^{\frac{3}{2}}}{2(1 + \sqrt{1-z})^2}.$$

Since this value is bounded for any  $\epsilon$  and  $R$ , we know that the smoothing error in  $\mathbb{R}^3$  converges to zero by either decreasing  $\epsilon$  or by increasing  $n$ . As in  $\mathbb{R}^1$ , we can provide an error estimate for the smoothing error. Let  $g(z) = \frac{1}{(1+\sqrt{1-z})^2}$ . Taylor's theorem tells us that

$$g(z) = \frac{1}{(1 + \sqrt{1-z})^2} = \sum_{i=1}^n \binom{-\frac{1}{2}}{i} (-1)^i \frac{1}{i+1} z^{i-1} + \frac{g^{(n)}(\xi)}{n!} z^n,$$

where  $\xi \in [0, z]$ . Hence,

$$\begin{aligned} \left| \sum_{i=n+1}^{\infty} \binom{-\frac{1}{2}}{i} (-1)^i \frac{1}{i+1} z^{i+\frac{1}{2}} \right| &= \left| \frac{z^{\frac{3}{2}}}{(1 + \sqrt{1-z})^2} - \sum_{i=1}^n \binom{-\frac{1}{2}}{i} (-1)^i \frac{1}{i+1} z^{i+\frac{1}{2}} \right| \\ &= \frac{|g^{(n)}(\xi)|}{n!} z^{n+\frac{3}{2}}. \end{aligned}$$

Since

$$\sum_{i=1}^{\infty} \binom{-\frac{1}{2}}{i} (-1)^i \frac{1}{i+1} = 1,$$

this gives

$$\sum_{i=n+1}^{\infty} \binom{-\frac{1}{2}}{i} (-1)^i \frac{1}{i+1} = 1 - \sum_{i=1}^n \binom{-\frac{1}{2}}{i} (-1)^i \frac{1}{i+1}.$$

This allows us to conclude that

$$\begin{aligned} e[n, \epsilon] &\leq \epsilon \rho_{\max} |S[n, \epsilon]| \\ &= \epsilon \rho_{\max} \left( \frac{2n+3}{2(n+1)} \binom{-\frac{1}{2}}{n} (-1)^n (z^{n+\frac{1}{2}} - 1) + \right. \\ &\quad \left. \frac{1}{2} \frac{|g^{(n)}(\xi)|}{n!} z^{n+\frac{3}{2}} - \frac{1}{2} \left( 1 - \sum_{i=1}^n \binom{-\frac{1}{2}}{i} (-1)^i \frac{1}{i+1} \right) \right). \end{aligned}$$

#### 4 Numerical Examples

Here we consider the Hamiltonian system with the Hamiltonian

$$H = \frac{1}{2} \sum_j \|\dot{\mathbf{x}}_j\|^2 - \sum_j \sum_{k \neq j} w_{jk} G(\mathbf{x}_j - \mathbf{x}_k),$$

where  $G$  is the free-space Green's kernel. Using Hamilton's equations, the acceleration of particle  $j$  is given by

$$\ddot{\mathbf{x}}_j = \sum_{k \neq j} w_{jk} \nabla_j G(\mathbf{x}_j - \mathbf{x}_k).$$

Since the Hamiltonian is a conserved quantity, it can be used to measure the accuracy of the time integrator. Because of the singularity in  $\nabla G$ , whenever two particles approach one another, the accuracy of the time integrator deteriorates, as we will see. Therefore, we will be taking the approach of using the regularized kernel with parameters  $\epsilon$  and  $n$ .

We will be reporting the error between the Hamiltonian of the regularized system and the Hamiltonian of the unregularized system. Specifically, the measured error is

$$\max_t |H^{\epsilon,n}(t) - H(0)| \leq \max_t |H^{\epsilon,n}(t) - H^{\epsilon,n}(0)| + |H^{\epsilon,n}(0) - H(0)|. \quad (12)$$

The first error term is due to truncation error when a discrete time integrator is used to approximate the solution; the second error term is the modelling error that arises from solving a regularized system. In a convergence study as  $\Delta t \rightarrow 0$ , the regularization error will eventually dominate the time stepping error—the overall error will plateau at the modelling error  $|H^{\epsilon,n}(0) - H(0)|$ . We first demonstrate the described behaviors in  $\mathbb{R}^1, \mathbb{R}^2$  and  $\mathbb{R}^3$  for a dynamical system with two particles of equal mass—one with a positive unit charge and the other with a unit negative charge. Two different sets of  $(\epsilon, n)$  pairings are used. Those in Table 1 keep the global smoothing error fixed at  $10^{-2}$ , as described in (11). The pairings reported in Table 2 keep the modelling error (9) fixed at  $4.89 \times 10^{-6}$ . Note that the modelling error depends on the initial condition whereas the global smoothing error does not. We conclude the numerical experiments by simulating 5 particles with an initial condition that results in a periodic orbit.

$n$	$\epsilon (\mathbb{R}^1)$	$\epsilon (\mathbb{R}^2)$	$\epsilon (\mathbb{R}^3)$
0	$7.9753 \times 10^{-4}$	$1.3022 \times 10^{-3}$	$6.2537 \times 10^{-4}$
1	$2.0001 \times 10^{-2}$	$3.0382 \times 10^{-2}$	$1.2038 \times 10^{-2}$
2	$5.2761 \times 10^{-2}$	$8.3471 \times 10^{-2}$	$3.1985 \times 10^{-2}$
4	$1.1366 \times 10^{-1}$	$1.8888 \times 10^{-1}$	$7.1597 \times 10^{-2}$
10	$2.3711 \times 10^{-1}$	$4.1171 \times 10^{-1}$	$1.5639 \times 10^{-1}$

Table 2: Values of  $\epsilon$  and  $n$  used in Figures 9, 13 and 16. Each pairing gives a regularized kernel that results in the same modelling error, equation (9), of  $4.89 \times 10^{-6}$ .

#### 4.1 Harmonic oscillator in $\mathbb{R}^1$

The unregularized system is simply

$$\ddot{x}_j = \frac{1}{2} \sum_{k \neq j} \begin{cases} -1 & x_j > x_k, \\ 1 & x_j < x_k. \end{cases}$$

We consider two particles initially located at -0.125 and 0.125. To break the symmetry of the problem, which can cause errors to cancel, we set the initial velocity of the left particle to be 0.1 and the right particle to be 0. Applying a fourth-order symplectic integrator, we see in Figure 7 that whenever the particles cross, there is a jump in the error of the Hamiltonian. This jump is caused by the lack of regularity of the derivative of the Green's function. If there are only a few particles, it is possible to exactly fix the jump in the Hamiltonian by using an adaptive time step size. However, this strategy is not possible for many particles, or in higher dimensions. As an alternative, we replace the singular kernel with a regularized kernel. While the jumps are still present when using a regularized kernel because of large derivatives, they are much smaller than those for the unregularized system.

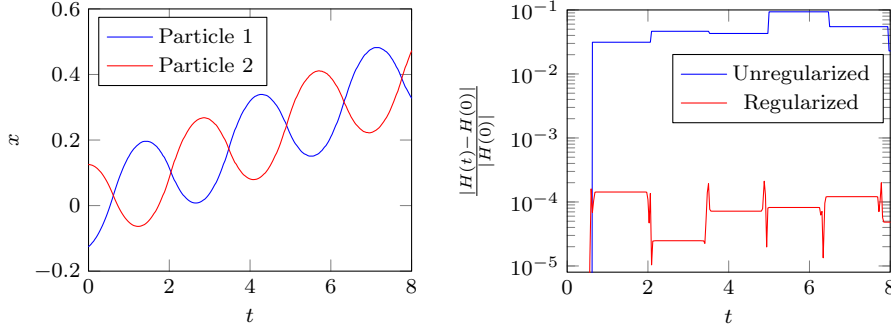


Fig. 7: The positions of the particles (left) and the errors in the Hamiltonian (right) when using the unregularized potential and regularized potential in  $\mathbb{R}^1$ . Time stepping was done with a fourth-order symplectic integrator. In this example, the time step size is  $3.125 \times 10^{-2}$  and the smoothing regularization parameter pairing is  $(\epsilon, n) = (5.6755 \times 10^{-2}, 10)$ .

While the use of regularized kernels reduces the size of the jumps in the Hamiltonian error, it does introduce a modelling error. In Figure 8, we plot the error in the Hamiltonian for six different regularizations: the unregularized kernel, and kernels regularized with the  $(\epsilon, n)$  pairings in Table 1. These pairings are specifically chosen because each  $(\epsilon, n)$  pair has the same global regularization error. For large  $\Delta t$ , there is no benefit for using the high-order regularized kernels. However, if smaller errors need to be achieved, then it is favorable to use a regularized kernel. Furthermore, we see that our new regularized kernels,  $n > 0$ , achieve smaller modelling errors, even though they have the same global smoothing error (10).

It could be argued that the regularization error can be simply decreased by taking a smaller value for  $\epsilon$  while keeping  $n$  fixed. However, if  $\epsilon$  is decreased, the



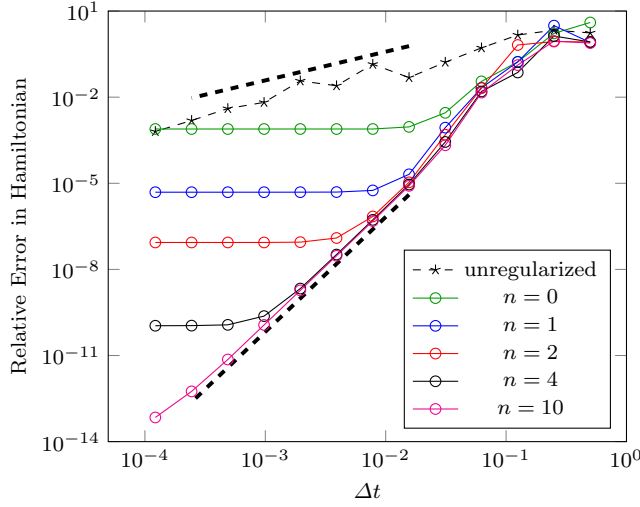


Fig. 8: The maximum Hamiltonian error (12) arising from evolving the regularized oscillator in  $\mathbb{R}^1$ , is studied as a function of  $\Delta t$ . While fourth-order convergence is eventually achieved for all  $(\epsilon, n)$  pairs from Table 1, the error eventually plateaus due to the modelling error of solving a regularized system. Although the  $(\epsilon, n)$  pairs have the same global regularization error, smaller modelling errors can be achieved when the higher-order kernels are used. The dashed black lines correspond to first- and fourth-order convergence.

derivative of the regularized kernel increases at the origin, and the result is a smaller asymptotic region for fourth-order convergence. In Figure 9, we compare the error in the Hamiltonian for  $(\epsilon, n)$  pairings that all have a modelling error of  $4.89 \times 10^{-6}$ . Using larger values of  $n$  results in larger regions of fourth-order convergence. The trade-off is the increased computational complexity for evaluating higher-order kernels.

Finally, we examine the phase plane of the variable  $z(t) = x_1(t) - x_2(t)$ . We increase the time horizon from  $T = 8$  to  $T = 400$  and keep the time step size fixed at  $3.125 \times 10^{-2}$ . In Figure 10, we plot the position  $z(t)$  versus the velocity  $\dot{z}(t)$  resulting from the unregularized potential and the regularized potential with  $n = 10, \epsilon = 5.6755 \times 10^{-2}$ ; the phase portrait when the other  $(\epsilon, n)$  pairings in Table 1 are indistinguishable in the eyeball norm from the  $n = 10$  kernel. The phase portrait of the unregularized system shows the effect of the truncation error due to a discrete time integrator being used in conjunction with the singular kernel. The qualitative periodic nature of the oscillations are perturbed. On the other hand, the regularized kernels allow significantly reduce the truncation error, better preserving the periodic nature of the orbits. If one were to compare the final solutions using the regularized kernels using the  $(\epsilon, n)$  pairings in Table 1, the errors would decrease with increasing  $n$  (not shown).

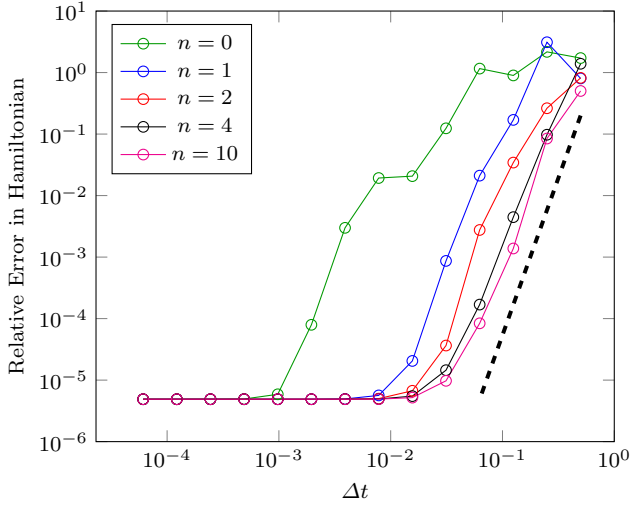


Fig. 9: The error in the Hamiltonian arising from using kernel regularization in  $\mathbb{R}^1$  with pairings of  $(\epsilon, n)$  in Table 2. Higher-order kernels have smoother transition regions, allowing for high-order convergence with larger time step sizes. The dashed black line corresponds to fourth-order convergence.

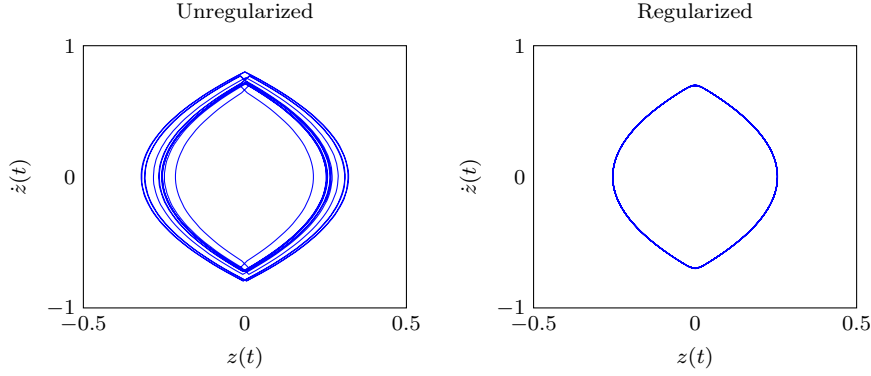


Fig. 10: The phase field of the  $z(t) = x_1(t) - x_2(t)$ . The regularized potentials maintain the periodic solution of the problem for coarse time steps.

#### 4.2 Harmonic oscillator in $\mathbb{R}^2$

Two particles are initially placed at  $(-0.25, 0)$  and  $(0.25, 0)$  with initial velocities  $(0, 10^{-3})$  and  $(0, 0)$  respectively. The unregularized system is

$$\ddot{\mathbf{x}}_j = \frac{1}{2\pi} \sum_{k \neq j} \frac{\mathbf{x}_j - \mathbf{x}_k}{|\mathbf{x}_j - \mathbf{x}_k|^2}.$$

These initial conditions were chosen so that the particles come close to each other without actually passing through each other. We expect the close proximity of the particles to each other to delay the fourth-order convergence if the unregularized system is solved. In Figure 11, the distance between the two particles and the error in the Hamiltonian as a function of time is plotted. When the particles are close to each other, there is a jump in the error of the Hamiltonian.

Repeating the numerical experiments from Section 4.1, Figure 12 shows the convergence behavior of the regularized dynamical system if the  $(\epsilon, n)$  pairings from Table 1 (fixed global smoothing error) are used. Similar observations to the experiment in  $\mathbb{R}^1$  can be observed: the symplectic integrator achieves fourth-order accuracy for each regularized system for large  $\Delta t$ , until the modeling error dominates. If the  $(\epsilon, n)$  pairings from Table 2 (fixed modelling error) are used, the higher-order regularized kernels exhibit fourth-order convergence for larger  $\Delta t$  (c.f. Figure 13).

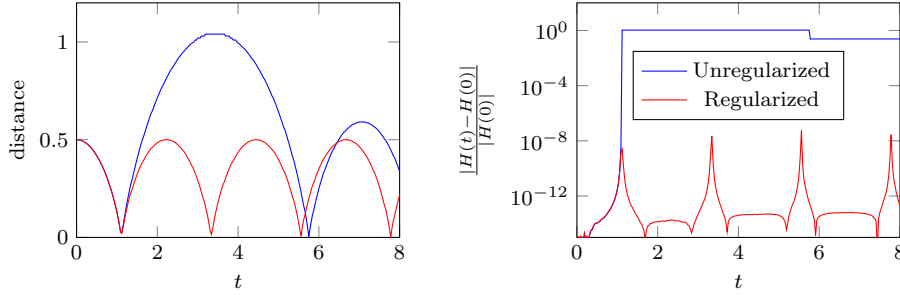


Fig. 11: The distance between the particles (left) and the errors in the Hamiltonian (right) when using the unregularized potential and regularized potential in  $\mathbb{R}^2$ . Time stepping was done with a fourth-order symplectic integrator. In this example, the time step size is  $4.88 \times 10^{-4}$  and the smoothing regularization parameter pairing is  $(\epsilon, n) = (3.6132 \times 10^{-2}, 10)$ .

#### 4.3 Harmonic oscillator in $\mathbb{R}^3$

Similarly, we place 2 particles at  $(-0.1, 0, 0)$  and  $(0.1, 0, 0)$  with initial velocities of  $(0, 10^{-3}, 0)$  and  $\mathbf{0}$  respectively. The unregularized system is

$$\ddot{\mathbf{x}}_j = \frac{1}{4\pi} \sum_{k \neq j} \frac{\mathbf{x}_j - \mathbf{x}_k}{|\mathbf{x}_j - \mathbf{x}_k|^3}.$$

As before, we expect that the singularity will reduce the order of accuracy of the fourth-order symplectic integrator. In fact, since the singularity is even stronger than in  $\mathbb{R}^2$ , we see that the unregularized system does not even obtain convergence for large  $\Delta t$  (Figure 15). By introducing a regularization, fourth-order convergence is observed. Again, as before, we observe that if the global smoothing error is kept constant, than larger values of  $n$  reduce the modelling error, and we are able to achieve more accurate results. As in  $\mathbb{R}^1$ , the benefit of using large values of  $n$  is illustrated in Figure 16. The modelling error is fixed at  $4.89 \times 10^{-6}$ , and the error in the Hamiltonian is plotted for the different  $(\epsilon, n)$  pairings.

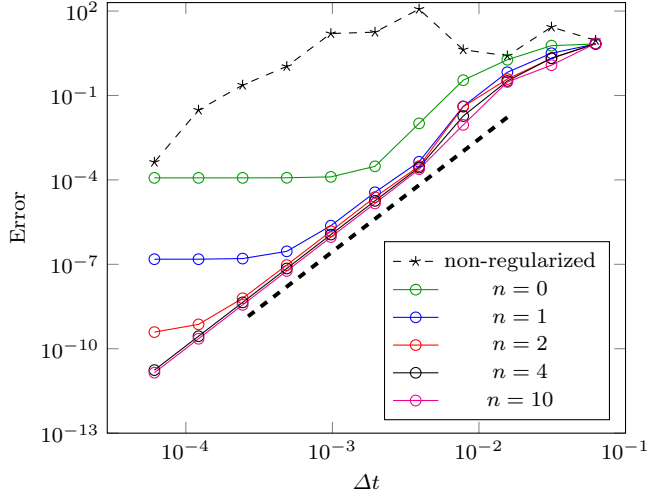


Fig. 12: The error in the Hamiltonian arising from using  $(\epsilon, n)$  pairings in Table 1 for the oscillator in  $\mathbb{R}^2$ . Fourth-order convergence is achieved for both the unregularized kernel and the regularized kernels. However, for the unregularized kernel, smaller time steps are required to enter this asymptotic regime. For the regularized systems, the error eventually plateaus when the modelling error dominates. By using larger values of  $n$ , smaller modelling errors can be achieved. The dashed black line corresponds to fourth-order convergence.

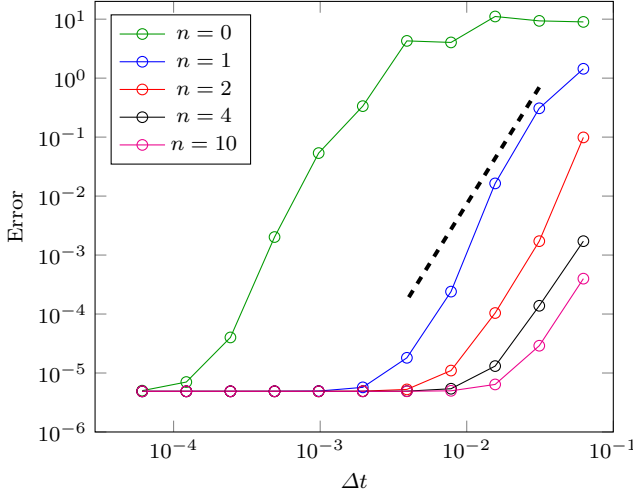


Fig. 13: The error in the Hamiltonian arising from using kernel regularization in  $\mathbb{R}^2$  with pairings of  $(\epsilon, n)$  that have the same modelling error of  $4.89 \times 10^{-6}$ . Larger values of  $n$  achieve desired accuracies with larger time step sizes. The dashed black line corresponds to fourth-order convergence.

#### 4.4 Periodic orbit in $\mathbb{R}^3$

We consider five particles in the  $z = 0$  plane of  $\mathbb{R}^3$ . We change the sign of  $G(r)$  so that the Hamiltonian system corresponds to motion due to the gravitational potential. By setting the mass of each particle to  $\sqrt{0.2}$ , so that  $w_{jk} = 2$ , and using

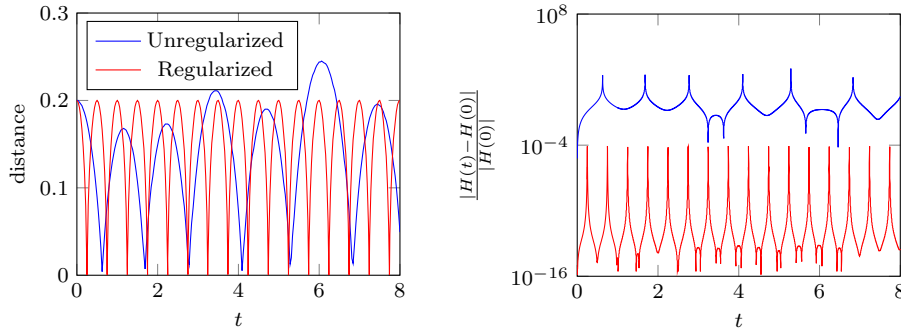


Fig. 14: The distance between the particles (left) and the errors in the Hamiltonian (right) when using the unregularized potential and regularized potential in  $\mathbb{R}^3$ . Time stepping was done with a fourth-order symplectic integrator. In this example, the time step size is  $2.44 \times 10^{-4}$  and the smoothing regularization parameter pairing is  $(\epsilon, n) = (2.8378 \times 10^{-2}, 10)$ .

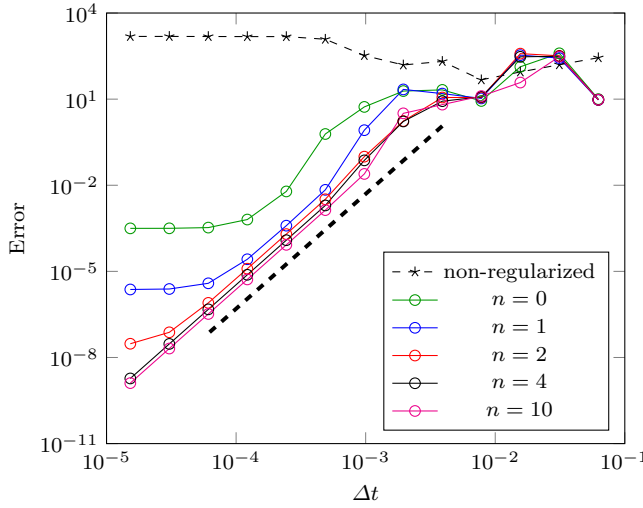


Fig. 15: The error in the Hamiltonian arising from using kernel regularization in  $\mathbb{R}^3$ . While fourth-order convergence is achieved for all values of  $n$ , the error eventually plateaus. By using larger values of  $n$ , smaller errors can be achieved. The dashed black line corresponds to fourth-order convergence.

the initial condition

$$\mathbf{x}(0) = \begin{pmatrix} +3.315332 \times 10^{-1} & 0 \\ +8.795500 \times 10^{-2} & -3.394340 \times 10^{-2} \\ -2.537216 \times 10^{-1} & -5.353020 \times 10^{-2} \\ -2.537216 \times 10^{-1} & +5.353020 \times 10^{-2} \\ +8.795500 \times 10^{-2} & +3.394340 \times 10^{-2} \end{pmatrix},$$

$$\dot{\mathbf{x}}(0) = \begin{pmatrix} 0 & -5.937860 \times 10^{-1} \\ +1.822785 \times 10^0 & +1.282480 \times 10^{-1} \\ +1.271564 \times 10^0 & +1.686450 \times 10^{-1} \\ -1.271564 \times 10^0 & +1.686450 \times 10^{-1} \\ -1.822785 \times 10^0 & +1.282480 \times 10^{-1} \end{pmatrix},$$

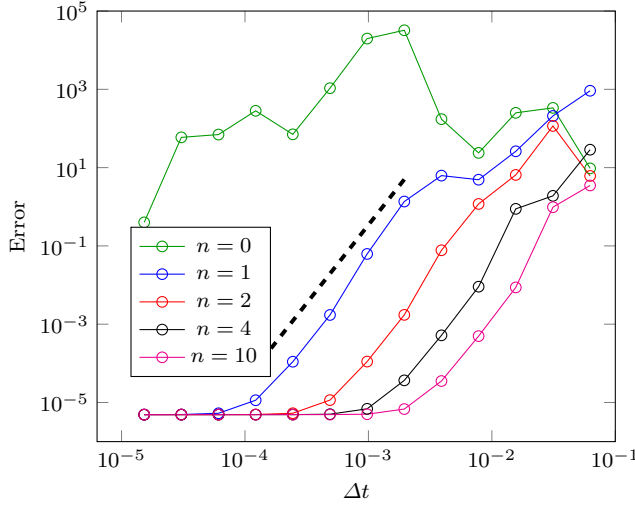


Fig. 16: The error in the Hamiltonian arising from using kernel regularization in  $\mathbb{R}^3$  with pairings of  $(\epsilon, n)$  that have the same regularization error of  $4.89 \times 10^{-6}$ . Larger values of  $n$  achieve desired accuracies with larger time step sizes. The dashed black line corresponds to fourth-order convergence.

the dynamics should result in a periodic orbit with period  $T = 2\pi/5$  [23]. Using a fourth-order symplectic integrator with  $10^6$  time steps, the non-regularized system does not give a periodic orbit, due to the singularity of the kernel. Using the  $(\epsilon, n)$  pairings from Table 1 (i.e., fixed global smoothing error), the orbits of the regularized system are shown in Figure 17. For the  $n = 0, 1, 2$  kernels, the modelling error dominates in the regularized system, resulting in orbits that are qualitatively different from the expected periodic orbit. The  $n = 4$  and  $n = 10$  kernels result in regularized systems that give qualitatively correct periodic orbits.

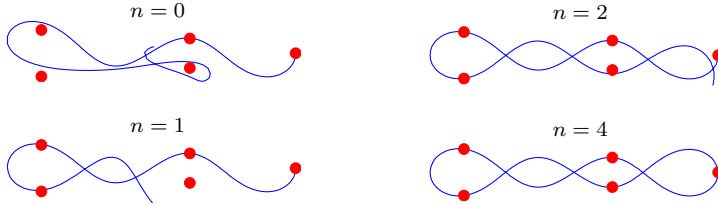


Fig. 17: The initial location of the five particles and the trajectory that one of the particles follows over one period. If  $n$  is too small, the correct orbit can not be achieved. However, with  $n = 4$ , the error in periodicity is  $10^{-2}$ . The orbit with  $n = 10$  looks similar to the orbit with  $n = 4$ .

The largest possible time step that keeps the relative error in periodicity bounded at  $10^{-2}$ , i.e.  $\|\mathbf{x}(T) - \mathbf{x}(0)\| < 10^{-2}\|\mathbf{x}(0)\|$ , is computed for the  $n = 4$  and  $n = 10$  systems. The results are reported in Table 3. A larger time step can be used for the  $n = 10$  kernels.

$n$	$\Delta t$	Period Error	Hamiltonian Error	Modelling Error
4	$1.58 \times 10^{-3}$	$9.99 \times 10^{-3}$	$3.65 \times 10^{-7}$	$2.50 \times 10^{-7}$
10	$2.29 \times 10^{-3}$	$9.98 \times 10^{-3}$	$5.13 \times 10^{-7}$	$9.87 \times 10^{-11}$

Table 3: A summary of the different errors when considering five particles that form a periodic orbit. We see that using  $n = 10$  allows for a larger time step size than  $n = 4$ .

## 5 Conclusions

In this paper, we derived a new family of regularized kernels, suitable for simulating a Hamiltonian system that contains the fundamental solution of Laplace’s equation using high-order time integrators. These high-order kernels were obtained by a Taylor expansion of the non-regularized kernel about  $(r^2 + \epsilon^2)$  in  $\mathbb{R}^1, \mathbb{R}^2$ , and  $\mathbb{R}^3$ . The analysis shows that the regularized kernels,  $G^{\epsilon, n}(r)$ , converge to the fundamental solution of Laplace’s equation as  $n \rightarrow \infty$  for any  $\epsilon > 0$ , and as  $\epsilon \rightarrow 0$  for any  $n \geq 0$ . In addition to the derivation and validation of the high-order kernels, error bounds for the regularized solution were derived.

We have shown that these regularizations can reduce the error in the far field without introducing sharp derivatives near the singularity. This is particularly useful when applying high-order time stepping methods to a Hamiltonian system such as a harmonic oscillator. In particular, high-order regularized kernels (with identical global smoothing error) can reduce the modelling error of the regularized system. Alternatively, if one chooses regularizations that give rise to similar modelling errors, high-order accuracy can be achieved for larger time step sizes using these high-order kernels.

Future work includes using these high-order kernels within treecode algorithms for approximating the electric field arising from a charged particle system [3, 4, 22]—this is necessary when simulating a large number of particles. In a treecode computation, a Taylor series expansion of the regularized potential is needed for the computation of the cluster-particle interaction. While explicit formulas for the Taylor coefficients of the high-order regularized kernels can be derived and evaluated, the computational complexity might be prohibitive. The authors anticipate that a recurrence relation to evaluate the Taylor coefficients of the high-order regularized kernels can be recovered. Certainly, the recurrence relation for the  $n = 0$  kernels are available [18]. Alternatively, a kernel-independent fast multipole method [20] can be used to significantly reduce the number of computations. With these fast algorithms, more complicated simulations such as vortex motions [14, 15] can be investigated. High-order regularized kernels can likely also be formulated in a similar fashion for the screened Coulomb potential [17] or Winckelmans–Leonard kernel [24].

## Acknowledgments

The authors would like to thank Robert Krasny, Keith Cartwright, John Verboncoeur, John Luginsland, Matthew Bettencourt, and Andrew Greenwood for their insightful discussions regarding this work.

## References

1. Bate, R.R., Mueller, D.D., White, J.E.: Fundamentals of astrodynamics. Courier Corporation (1971)
2. Beale, J.: A grid-based boundary integral method for elliptic problems in three dimensions. *SIAM Journal on Numerical Analysis* **42**(2), 599–620 (2004)
3. Christlieb, A., Krasny, R., Verboncoeur, J.: A treecode algorithm for simulating electron dynamics in a Penning–Malmberg trap. *Computer Physics Communications* **164**(1–3), 306–310 (2004)
4. Christlieb, A., Krasny, R., Verboncoeur, J.: Efficient particle simulation of a virtual cathode using a grid-free treecode Poisson solver. *Plasma Science, IEEE Transactions on* **32**(2 Part 1), 384–389 (2004)
5. Christlieb, A., Krasny, R., Verboncoeur, J., Emhoff, J., Boyd, I.: Grid-free plasma simulation techniques. *Plasma Science, IEEE Transactions on* **34**(2 Part 1), 149–165 (2006)
6. Cortez, R.: The Method of Regularized Stokeslets. *SIAM Journal on Scientific Computing* **23**(4), 1204–1225 (2001)
7. Cortez, R., Minion, M.: The blob projection method for immersed boundary problems. *Journal of Computational Physics* **161**(2), 428 – 453 (2000). DOI <http://dx.doi.org/10.1006/jcph.2000.6502>. URL <http://www.sciencedirect.com/science/article/pii/S0021999100965021>
8. Faou Erwanand Hairer, E., Pham, T.L.: Energy conservation with non-symplectic methods: Examples and counter-examples. *BIT Numerical Mathematics* **44**(4), 699–709 (2004). DOI [10.1007/s10543-004-5240-6](https://doi.org/10.1007/s10543-004-5240-6). URL <http://dx.doi.org/10.1007/s10543-004-5240-6>
9. Forest, E., Ruth, R.D.: Fourth-order symplectic integration. *Phys. D* **43**(1), 105–117 (1990). DOI [10.1016/0167-2789\(90\)90019-L](https://doi.org/10.1016/0167-2789(90)90019-L). URL [http://dx.doi.org/10.1016/0167-2789\(90\)90019-L](http://dx.doi.org/10.1016/0167-2789(90)90019-L)
10. Gibbon, P., Speck, R., Karmakar, A., Arnold, L., Frings, W., Berberich, B., Reiter, D., Masek, M.: Progress in Mesh-Free Plasma Simulation With Parallel Tree Codes. *Plasma Science, IEEE Transactions on* **38**(9), 2367–2376 (2010)
11. Hejlesen, M.M., Rasmussen, J.T., Chatelain, P., Walther, J.H.: A high order solver for the unbounded Poisson equation. *J. Comput. Phys.* **252**, 458–467 (2013). DOI [10.1016/j.jcp.2013.05.050](https://doi.org/10.1016/j.jcp.2013.05.050). URL <http://dx.doi.org/10.1016/j.jcp.2013.05.050>
12. Hosseini, B., Nigam, N., Stockie, J.M.: On regularizations of the Dirac delta distribution. *J. Comput. Phys.* **305**, 423–447 (2016)
13. Jackson, J.D.: Classical electrodynamics. Wiley (1999)
14. Krasny, R.: Desingularization of periodic vortex sheet roll-up. *Journal of Computational Physics* **65**(2), 292–313 (1986)
15. Krasny, R.: Computation of vortex sheet roll-up in the Trefftz plane. *Journal of Fluid Mechanics* **184**, 123–155 (1987)
16. Leonard, A.: Vortex methods for flow simulation. *J. Comput. Phys.* **37**(3), 289–335 (1980). DOI [10.1016/0021-9991\(80\)90040-6](https://doi.org/10.1016/0021-9991(80)90040-6). URL [http://dx.doi.org/10.1016/0021-9991\(80\)90040-6](http://dx.doi.org/10.1016/0021-9991(80)90040-6)
17. Li, P., Johnston, H., Krasny, R.: A cartesian treecode for screened coulomb interactions. *Journal of Computational Physics* **228**(10), 3858 – 3868 (2009). DOI <http://dx.doi.org/10.1016/j.jcp.2009.02.022>. URL <http://www.sciencedirect.com/science/article/pii/S0021999109000916>
18. Lindsay, K., Krasny, R.: A particle method and adaptive treecode for vortex sheet motion in three-dimensional flow. *Journal of Computational Physics* **172**(2), 879–907 (2001)
19. Majda, A., Majda, G., Zheng, Y.: Concentrations in the one-dimensional Vlasov-Poisson equations, I: Temporal development and non-unique weak solutions in the single component case. *Physica D* **74**(3–4), 268–300 (1994)
20. Rostami, M.W., Olson, S.D.: Kernel-Independent Fast Multipole Method within the framework of Regularized Stokeslets. *Journal of Fluids and Structures* (2015). Under review
21. Ruth, R.D.: A canonical integration technique. *IEEE Transactions on Nuclear Science* **30**(4), 2669–2671 (1983). DOI [10.1109/TNS.1983.4332919](https://doi.org/10.1109/TNS.1983.4332919)
22. Salmon, J., Warren, M.: Skeletons from the treecode closet. *Journal of Computational Physics* **111**(1), 136–155 (1994)
23. Simó, C.: New families of solutions in N-body problems. In: *European Congress of Mathematics*, pp. 101–115. Springer (2001)



- 
24. Wee, D., Marzouk, Y.M., Schlegel, F., Ghoniem, A.F.: Convergence characteristics and computational cost of two algebraic kernels in vortex methods with a tree-code algorithm. *SIAM J. Sci. Comput.* **31**(4), 2510–2527 (2009). DOI 10.1137/080726872. URL <http://dx.doi.org/10.1137/080726872>
  25. Winckelmans, G.S., Leonard, A.: Contributions to vortex particle methods for the computation of three-dimensional incompressible unsteady flows. *J. Comput. Phys.* **109**(2), 247–273 (1993). DOI 10.1006/jcph.1993.1216. URL <http://dx.doi.org/10.1006/jcph.1993.1216>